Journal of Solid State Chemistry 183 (2010) 3058–3066

Contents lists available at ScienceDirect

Journal of Solid State Chemistry

journal homepage: www.elsevier.com/locate/jssc

Unprecedented solid-state chemical reaction—from $(C_3N_2H_5)_3SbBr_6 \cdot H_2O$ to $(C_3N_2H_5)_5Sb_2Br_{11}$. From centrosymmetric to non-centrosymmetric crystal structure

A. Piecha [a], A. Gągor [b], A. Pietraszko [b], R. Jakubas [a,*]

[a] Faculty of Chemistry, University of Wrocław, Joliot–Curie 14, 50-383 Wrocław, Poland
[b] Institute of Low Temperature and Structure Research, Polish Academy of Science, Okólna 2, 50 - 950 Wrocław 2, PO Box 937, Poland

ARTICLE INFO

Article history:
Received 30 April 2010
Received in revised form
5 October 2010
Accepted 16 October 2010
Available online 23 October 2010

Keywords:
Halogenoantimonates(III)
Phase transition
Hydrogen bonds
Ferroelectric hybrid materials

ABSTRACT

Tris(imidazolium) hexabromoantimonate(III) hydrate, $(C_3N_2H_5)_3SbBr_6 \cdot H_2O$, (abbreviated as TIBA) has been synthesized and characterized by X-ray (at 295, 225, 160, and 110 K), differential scanning calorimetry, dilatometry, and dielectric spectroscopy. At room temperature (phase I), the structure consists of discrete SbB_6^- anions, disordered imidazolium cations, and water molecules forming a 3D array of hydrogen bonds. Below room temperature, TIBA was found to undergo isostructural discontinuous phase transition at 212/221 K (cooling–heating) ($P2_1/c \leftrightarrow P2_1/c$). The phase transition mechanism is characterized by two contributions: an order–disorder (cationic substructure) and a displacive (water molecules) one. At high temperatures, the TIBA crystal was found to undergo an unprecedented in situ solid-state chemical reaction:

$$2(C_3N_2H_5)_3SbBr_6 \cdot H_2O_{(S)} \rightarrow (C_3N_2H_5)_5Sb_2Br_{11(S)} + (C_3N_2H_5)Br_{(S)} + 2H_2O \quad (1)$$

This chemical transformation leads to multiphase crystallites dominated by an amorphous phase of $(C_3N_2H_5)_5Sb_2Br_{11}$. The creation of ferroelectric crystallites – $(C_3N_2H_5)_5Sb_2Br_{11}$ – in an "annealed" sample of $(C_3N_2H_5)_3SbBr_6 \cdot H_2O$ was confirmed by X-ray diffraction phase analysis, dielectric spectroscopy, and pyroelectric measurements. The dielectric response of the electric permittivity and the critical slowing down of the process observed near 140 K in the "annealed" sample of TIBA are treated as a "fingerprint" of a neat $(C_3N_2H_5)_5Sb_2Br_{11}$ ferroelectric.

1. Introduction

Nonlinear optical (NLO) and nonlinear dielectric (ferroelectric, piezoelectric) materials have recently been attracting much attention because they may be widely used in advanced laser technology, optoelectronics, optical storage and information processing, as well as mechanical energy transfer [1–8]. Ferroelectric properties have been discovered in numerous halogenoantimonates(III) and halogenobismuthates(III) forming molecular-ionic crystals of the general formula $R_aM_bX_{3b+a}$ (where R denotes organic cations, M = Sb, Bi and X = Cl, Br, I) [9–11]. A characteristic feature of these molecular-ionic solid complexes is a rich diversity of anionic substructures [12,13]. So far, more than 30 various anionic frameworks have been synthesized. However, ferroelectricity is limited to compounds crystallizing with the chemical compositions $R_3M_2X_9$ [14,15] and $R_5M_2X_{11}$ [16–18], where R stands for dipolar organic cations.

The cations usually occupy large vacancies inside the anionic substructures. The dynamics of the cations is believed to contribute to dielectric permittivity close to the Curie temperature and to spontaneous polarization. The role of the anionic framework in the induction of ferroelectricity remains unclear. It is suggested that the lone pair ($5s^2$—Sb(III) and $6s^2$—Bi(III)) has a key role in the collective properties of these ferroelectric materials [11]. Recently, we have synthesized three novel ferroelectrics from the haloantimonate(III) and halobismuthate(III) family of compounds crystallizing with the chemical composition $R_5M_2X_{11}$, where R is the imidazolium cation [19,20]. It is rather intriguing that all known compounds (imidazolium, pyridinium, or methylammonium cations) with this composition have been found to exhibit ferroelectric properties, whereas formally very similar compounds crystallizing with H_2O molecules, $(R_5M_2X_{11} \cdot 2H_2O)$, do not reveal any ferroelectric properties [21,22]. Since R_3MX_6 derivatives had previously not been studied in any systematic way, we extended

* Corresponding author.
E-mail address: rj@wchuwr.pl (R. Jakubas).

0022-4596/$ - see front matter © 2010 Elsevier Inc. All rights reserved.
doi:10.1016/j.jssc.2010.10.020

our structural, thermal, and dielectric studies to molecular-ionic salts characterized by this chemical composition. Compounds with the R_3MX_6 composition consist of isolated octahedra and usually feature the simplest anionic framework in the described family of crystals [23–27]. Ferroic properties have hitherto not been found in compounds crystallizing with the R_3MX_6 composition, in contrast to $R_3M_2X_9$ and $R_5M_2X_{11}$-type derivatives.

A novel organic–inorganic hybrid material, tris(imidazolium) hexabromoantimonate(III) hydrate, $(C_3N_2H_5)_3SbBr_6 \cdot H_2O$ (abbreviated as TIBA), has been synthesized. In this paper we report single-crystal X-ray and powder X-ray diffraction, calorimetric, dilatometric, dielectric and pyroelectric studies on this compound over a wide range of temperatures. A possible mechanism of low-temperature structural phase transition in TIBA is discussed. An unusual solid-state chemical reaction above room temperature (328 K) that leads from $[SbBr_6]^{3-}$ to $[Sb_2Br_{11}]^{5-}$ chemical stoichiometry of anions is postulated to take place in TIBA. Direct experimental evidence for the presence of crystalline phase of $(C_3N_2H_5)_5Sb_2Br_{11}$ (a ferroelectric compound [20]) as a final product of the solid-state chemical reaction of TIBA decomposition is presented and discussed.

2. Experimental

The starting materials for the synthesis of imidazolium bromoantimonate(III); $(C_3N_2H_5)_3SbBr_6 \cdot H_2O$ were commercial $SbBr_3$ (99.999%, Aldrich), imidazole amine—$C_3N_2H_4$ (99.5%, Fluka) and HBr (48%, Sigma-Aldrich). To a solution of antimony(III) bromide in 48% aqueous of hydrobromic acid an aqueous solution of imidazolium bromide was added. The resulting yellow precipitate was redissolved by heating and on cooling gave dark yellow polycrystals. *Analysis*: *found*: C—8.02%, N—6.21%, H—1.16%; *calc*., C—8.04%, N—6.25%, H—1.12%). Single crystals were grown from an aqueous solution by slow evaporation at constant room temperature 295 K.

Differential scanning calorimetry (DSC) was recorded using a Perkin Elmer DSC-7 in the temperature range 100–450 K.

The complex electric permittivity $\varepsilon^* = \varepsilon' - i\varepsilon''$ was measured between 100 and 370 K by the Agilent 4284A Precision LCR Meter in the frequency range between 2 kHz and 1 MHz. The dimensions of the sample were approximately of $4 \times 4 \times 1$ mm^3. The overall error was less than 5%.

The spontaneous polarization was measured between 100 and 250 K by a charge integration technique using a Keithley 617 Programmable Electrometer. The temperature was stabilized by an Instec STC 200 temperature controller.

A single-crystal X-ray diffraction experiments were performed on a Kuma KM4CCD diffractometer using a graphite monochromated Mo Kα radiation. An open flow nitrogen cryosystem (Oxford Cryosystem) was used for experiments from 100 to 300 K. Thermal evolution of lattice parameters was measured from 100 to 300 K with a step 10–15 K. Lattice parameters were obtained by a least square fit to 1 1 0 reflections. The CrysAlis software version 1.170.32 [29] was used for data processing. An empirical absorption correction was applied using spherical harmonics implemented in SCALE3 ABSPACK scaling algorithm. The structure was solved by direct methods and refined by the full-matrix least-squares method by means of SHELX-97 program package [30]. All measurements were carried out on the same crystal specimen.

Powder diffraction data were collected at X'Pert PRO X-ray Diffraction system equipped with PIXcel ultra-fast line detector for Cu Kα radiation, focusing mirror and Soller slits. The samples were prepared in a glass capillaries of 0.7 mm. The high-temperature measurements were done using Anton Paar 1200 N High-Temperature Oven Chamber.

3. Results and discussion

3.1. Thermal properties of $(C_3N_2H_5)_3SbBr_6 \cdot H_2O$ (TIBA); DSC, DTA, TGA

The DSC curves obtained for TIBA on cooling and heating scans below room temperature (RT) are presented in Fig. 1(a). The compound reveals one heat anomaly at 212/221 K (on cooling/heating), attributed to a discontinuous (first order) structural phase transition, which is perfectly reversible. The entropy of transition, ΔS_{tr}, accompanying the I → II phase transition was found to be rather large, *ca*. 14.6 J/mol K. Transition entropy (ΔS_{tr}) is characteristic of an order–disorder phase transition mechanism. The X-ray results presented below show that there are three types of imidazolium cations in the crystal lattice. Experimentally observed ΔS_{tr} can be interpreted in terms of Boltzmann's principle: $\Delta S = 3\ \ln(N1/N2)$, where $N1$ and $N2$ are the number of distinguishable orientations allowed in the high-temperature and the low-temperature phases, respectively. The observed value of 14.6 J/mol K leads to $N\,1/N2 \approx 1.8$. It means that if the three imidazolium cations are ordered in the low-temperature phase, they should be distributed over two sites in the room-temperature (RT) phase.

Above RT, the compound showed a huge heat anomaly (ΔH), *ca*. 3640 J/mol ($\Delta S = 111$ J/mol K) at 328 K, which is characteristic of a chemical process. The chemical transformation appeared to be irreversible, as expected. Thermal stability of the crystal was studied by means of simultaneous thermogravimetric analysis (TGA) and differential thermal analysis (DTA) between 300 and 700 K. The results, presented in Fig. 1(b), show that $(C_3N_2H_5)_3SbBr_6 \cdot H_2O$ exhibits one endothermal peak at about 325 K on the DTA curve, which corresponds to the high-temperature heat anomaly detected at 328 K by the DSC method. The crystal seems to be stable up to about 320 K, and above this temperature a continuous weak loss of sample mass takes place. Further heating of the sample is accompanied by a weak endotherm at 358 K and a strong one at *ca*. 475 K. Above 540–550 K, the sample decomposes rapidly. Fig. 1(b) shows that between 320 and 335 K, the mass loss of the sample is not larger than 0.7%, which could suggest that the sample is still stable. The various experimental methods presented in this paper showed, however, that in this temperature range we deal with a solid-state chemical process.

On the basis of the results of thermogravimetric analysis, the following chemical reaction is proposed in the temperature range from 320 to 340 K:

$$2(C_3N_2H_5)_3SbBr_6 \cdot H_2O_{(S)} \rightarrow (C_3N_2H_5)_5Sb_2Br_{11(S)} + (C_3N_2H_5)Br_{(S)} + 2H_2O \quad (2)$$

Further heating of the sample leads to a weak endotherm at 358 K, which is assigned to the structural phase transition detected in the neat ferroelectric $(C_3N_2H_5)_5Sb_2Br_{11}$ at 354 K [20]. Before full decomposition of the sample occurs (above 540–550 K), a decay of $(C_3N_2H_5)Br_{(s)}$ probably takes place:

$$(C_3N_2H_5)Br_{(s)} \rightarrow \tfrac{1}{2}Br_{2(g)} + C_3N_2H_{5(g)} \quad (3)$$

We focused our attention on the first stage of the chemical process taking place in our sample; thus, detailed analysis of the thermal situation above 380–400 K is beyond our interests. What is most intriguing is that the in situ chemical process taking place in the solid state at 328 K leads to a ferroelectric crystalline compound given by the formula $(C_3N_2H_5)_5Sb_2Br_{11}$. The possibility of the existence of a ferroelectric order at low temperatures in an "'annealed" sample was confirmed by the dielectric results.

Since $(C_3N_2H_5)Br_{(s)}$ is one of the products of reaction (2), we decided to synthesize $(C_3N_2H_5)Br_{(s)}$ and evaluate its thermal properties in order to compare them with those obtained for TIBA and $(C_3N_2H_5)_5Sb_2Br_{11}$. Polycrystals of $(C_3N_2H_5)Br_{(s)}$, which

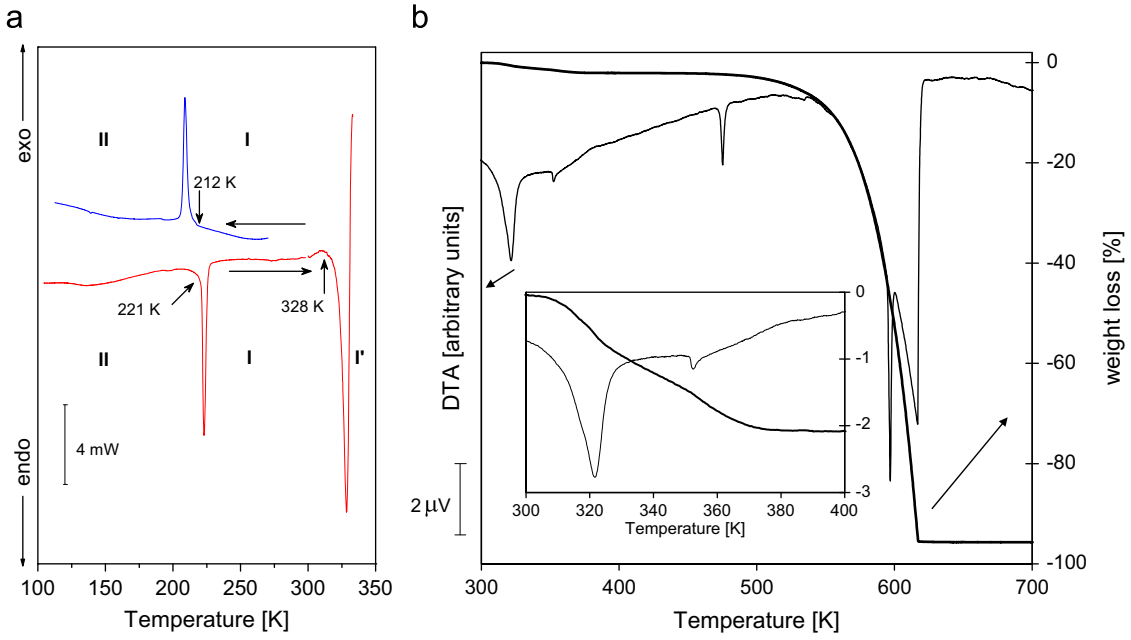

Fig. 1. (a) DSC curves for the $(C_3N_2H_5)_3SbBr_6 \cdot H_2O$ crystal upon cooling and heating (10 K/min, $m = 14.3$ mg). (b) Simultaneous TGA and DTA thermograms between 300 and 700 K.

appeared to be extremely hygroscopic, were kept at 350 K for several hours and then calorimetric measurements were performed. The sequence of phase transitions seems to be rather complex because two thermal anomalies were found on cooling and three on heating. For the sake of brevity of this paper, we do not discuss these results in detail. The fact that appeared to be the most important for us was that $(C_3N_2H_5)Br_{(s)}$ underwent discontinuous transition at about 194/198 K (cooling–heating), which was not characteristic of $(C_3H_5N_2)_3SbBr_6 \cdot H_2O$ or neat $(C_3N_2H_5)_5Sb_2Br_{11}$. It should be emphasized, that thermal and dielectric properties for $(C_3N_2H_5)Br_{(s)}$ are presented for the first time.

3.2. Single-crystal X-ray diffraction of TIBA: room and low-temperature phases

Table 1 summarizes data collection and reduction and structural parameters at selected temperatures. Since all important differences were found between the structures at 295 and 225 K in phase I and at 160 and 110 K in phase II, the further discussion is based on the data for 225 and 160 K, respectively. Structural results at 295 and 110 K are given in Supplementary Materials (Table 1).

TIBA crystallizes in the monoclinic system, space group $P2_1/c$. The asymmetric unit contains three independent imidazolium cations and an $[SbBr_6]^{3-}$ anion. A perspective view of the arrangement of these constituent ions at 225 K is shown in Fig. 2(a) together with the atom numbering scheme. All atoms occupy general positions with C_1 symmetry. All the nitrogen and carbon atoms that build imidazolium rings exhibit considerable thermal motion in phase I, which points to orientational disorder of those cations. While imidazolium cations A and B perform most probably only the small-angle libration motion reflected in the elongated atomic displacement parameters within the plane of the ring, imidazolium cation *C* is able to perform a 180° reorientation within the plane of the pentagonal ring. The splitting atom model was used to represent the disorder of cation C.

Fig. 2(a) shows also two possible orientations of imidazolium cation C-type at 225 K. Both were chosen in a way that introduced the best geometry of N−H···Br bonds. The presented model with two independent orientations properly reflects the electron density map; however, other orientations of these cations are also probable since the discrepancy factor *R* rose only slightly when other orientations were examined.

Table 1
Crystal data and structure refinement for $(C_3N_2H_5)_3SbBr_6 \cdot H_2O$ at 225 and 160 K.

Phase	225 K	160 K
Chemical formula	$C_9H_{17}Br_6N_6OSb$	$C_9H_{17}Br_6N_6OSb$
M_r	826.5	826.5
Cell setting, space group	Monoclinic, $P2(1)/c$	
Temperature (K)	225(2)	160(2)
a (Å)	8.7600(4)	8.9137(4)
b (Å)	19.8559(10)	19.2032(5)
c (Å)	13.0231(7)	12.7984(5)
β(°)	90.707(4)	90.650(5)
V (Å^3), Z	2265.0, 4(7)	2190.58, 4
D_x (Mg M^{-3})	2.409	2.506
Data collection		
No. of measured, independent and observed reflections	23 597, 5303, 3486	22 710, 5147, 3716
Criterion for observed reflections	$I > 2\sigma(I)$	
R_{int}, Θ_{max} (°)	0.031, 28.2	0.044, 28.3
Refinement		
Refinement on	F^2	
$R[F^2 > 2\sigma(F^2)]$, $wR(F^2)$, S	0.021, 0.033, 0.84	0.024, 0.049, 0.91
No. of reflections	5303	5147
No. of parameters	211	214
$(\Delta/\sigma)_{max}$	0.021	0.003
$\Delta\rho_{max}$, $\Delta\rho_{min}$ (eÅ^{-3})	0.53, −0.56	0.96, −0.71

The anionic substructure consists of discrete $SbBr_6$ octahedra with three shorter contacts (mean Sb–Br distance of 2.69 Å) and three weaker contacts (mean Sb–Br distance of 2.96 Å). The geometry of the anion is characteristic of compounds with the general formula R_3MX_6 that possess an anionic substructure composed of isolated octahedra [28].

Fig. 2(b) illustrates the most important details of molecular crystal packing of $(C_3N_2H_5)_3SbBr_6 \cdot H_2O$ at 225 K, in phase I. The minimum separation distance between Sb positions is 7.8648(3) Å.

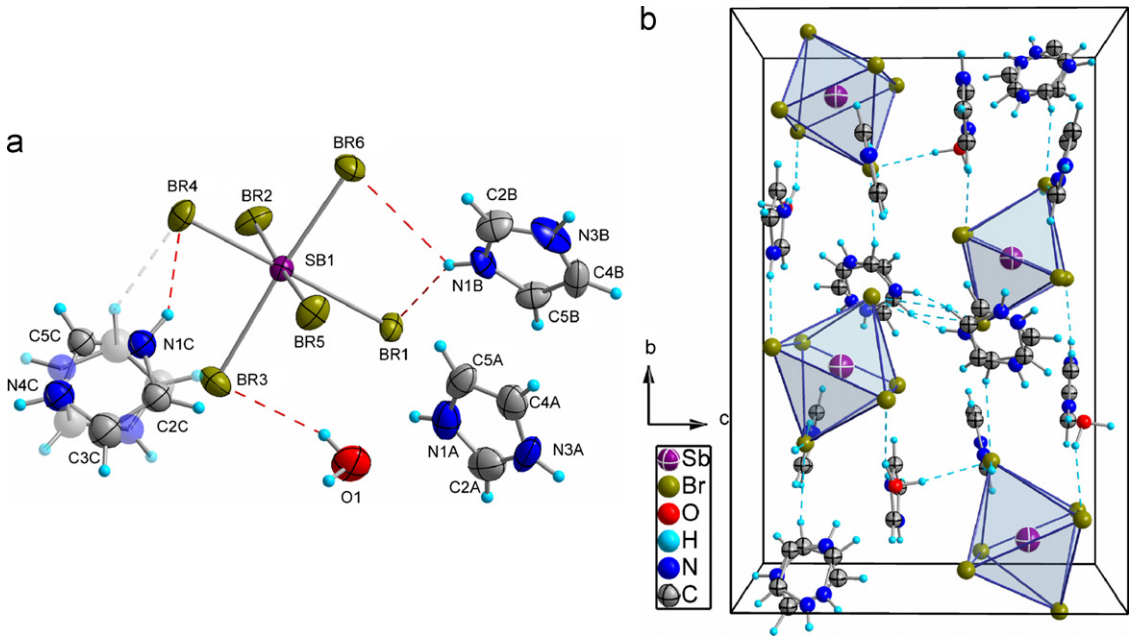

Fig. 2. (a) Asymmetric unit content in $(C_3N_2H_5)_3SbBr_6 \cdot H_2O$. Thermal ellipsoids are plotted at 50% probability level, T=225 K. (b) The projection of $(C_3N_2H_5)_3SbBr_6 \cdot H_2O$ crystal packing along the a-direction, phase I, T = 225 K. Thermal ellipsoids are plotted at 50% probability level. Blue dashed lines represents hydrogen bonds. (For interpretation of the references to colour in this figure legend, the reader is referred to the web version of this article.)

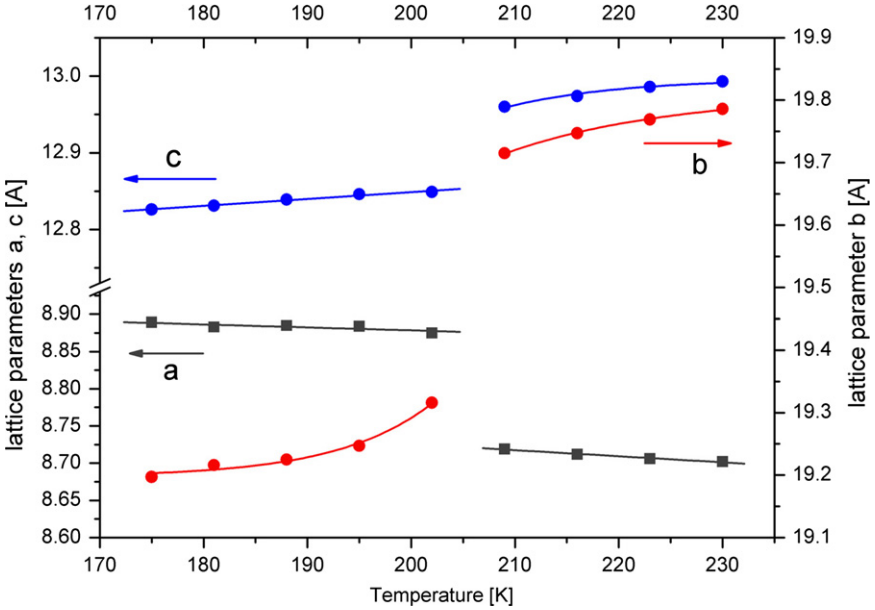

Fig. 3. Thermal evolution of lattice parameters in $(C_3N_2H_5)_3SbBr_6 \cdot H_2O$ on cooling. Standard deviations are comparable to the points marked in the picture.

$(C_3N_2H_5)_3SbBr_6 \cdot H_2O$ undergoes discontinuous (first order) phase transition at 212 K. All cell parameters show abrupt changes at this temperature; they are most pronounced for directions a and b ($\Delta a/a = 0.018$, $\Delta b/b = 0.02$, $\Delta c/c = 0.009$); see Fig. 3. The β-angle does not change significantly. The phase transition is isostructural; the metrics and the symmetry remain the same, $P2_1/c$, over the whole low-temperature range. The most strongly affected by the transition are imidazolium rings C, which order below 212 K. However, the effect on the H_2O position is also striking. In phase I at 225 K, the water molecule interacts with two bromine ions (Br1 and Br3) from two different octahedra *via* hydrogen bonds. Additionally, oxygen O1 serves as an acceptor for two hydrogen atoms from imidazolium A and C, namely N1A–H1A···O1 with the donor–acceptor distance of 2.904(2) Å and N11C–H11C···O1 with the donor–acceptor distance of 3.142(4) Å (Tables 2 and 3 in Supporting Materials). After the phase transition, the water molecule moves towards the Br2 atom and imidazolium cation C (see Fig. 1 in Supporting Materials). The distances O1–Br2 and O1–N3C change significantly: from 3.882 to 3.532 Å and from 3.206 to 2.821 Å, respectively. In this way, in the low-temperature phase a new bifurcated hydrogen bond appears: O1–H2···Br2 and O1–H2···Br1 with donor–acceptor distances of 3.529(2) and 3.222(2) Å at 160 K, respectively.

The geometrical parameters, such as bond distances and angles in the anionic substructure, seem to be less affected. However, one

significant distortion should be emphasized: after the phase transition, the Br2–Sb–Br3 angle increases significantly, from 91.87° to 98.69°. This deformation arises as a result of much stronger hydrogen interactions between water and the Br2, Br3 bromine atoms in the low-temperature phase. The shift of the water molecule and the deformation of the $SbBr_6$ octahedra, probably simultaneous, entail abrupt changes of the unit cell parameters at the phase transition. Table 2 presents the Sb–Br distances above and below the phase transition temperature (212 K). The values change only slightly; the largest change (increase), by 0.093 Å, is observed for the Sb–Br1 distance.

In both phases, the imidazolium rings and water molecules interact with the anionic substructure forming a 3D array of hydrogen bonds. In phase I, imidazolium B serves to bridge two neighboring $SbBr_6$ octahedra via N−H···Br bonds, namely, N1B−H1B···Br1 and N3B−H3B···Br1 with donor–acceptor distances of 3.315(2) and 3.369(9) Å, respectively. Imidazolium A interacts with only one anion, *via* the N3A−H3A···Br2 bond with a donor–acceptor distance of 3.384(2) Å. Additionally, a second nitrogen atom, N1A, acts as an acceptor for hydrogen from the water molecule. The disordered imidazolium C also interacts with the anionic substructure, though the possible hydrogen bonds must have an instantaneous character according to the dynamical reorientation of the imidazolium ring. Significantly, the bromine atom Br1 acts as threefold hydrogen-bonded acceptor from two cations (B and C) and the water molecule, whereas the atoms Br2, Br3, Br4 are acceptors for two hydrogens, one from imidazolium A (N1A) and the other from the disordered imidazolium C (N11C). Details of the geometry of the hydrogen bonding interactions are gathered in Table 3. After the phase transition, the strength of the hydrogen bonds does not change significantly. Instead, additional short contacts, N1A−H1A···Br5 and N1B−H1B···Br6, appear, with a mean donor–acceptor distance of 3.519(2) Å. Also, a tendency to improve the geometry of the hydrogen bonds is observed (Tables 3 and 2 in Supporting Materials).

Table 2
Sb–Br distances at 225 and 160 K in $(C_3N_2H_5)_3SbBr_6 \cdot H_2O$.

	225 K	160 K
Sb(1)–Br(1)	2.9914(3)	2.8983(3)
Sb(1)–Br(2)	2.9713(3)	3.0038(4)
Sb(1)–Br(3)	2.9192(3)	2.9205(4))
Sb(1)–Br(4)	2.6768(3)	2.7210(3)
Sb(1)–Br(5)	2.6907(3)	2.6648(4)
Sb(1)–Br(6)	2.7040(3)	2.6926(4)

Table 3
Hydrogen bonding interactions in $(C_3N_2H_5)_3SbBr_6 \cdot H_2O$.

D−H···A	d(D–H)	d(H···A)	d(D···A)	<(DHA)
225 K				
N(1B)−H(1B)···Br(1)	0.86	2.59	3.3154(15)	143.1
N(1C)−H(1C)···Br(4)	0.89	2.73	3.493(3)	144.6
N(41C)−H(41C)···Br(3)	0.83	2.91	3.636(4)	147.6
N(11C)−H(11C)···O(1)	0.85	2.42	3.142(4)	143.4
N(1A)−H(1A)···O(1)	0.86	2.15	2.904(2)	146.0
N(4C)−H(4C)···Br(2)	0.88	2.62	3.489(3)	172.0
N(3A)−H(3A)···Br(2)	0.86	2.54	3.3835(18)	168.7
N(3B)−H(3B)···Br(1)	0.86	2.52	3.3692(19)	168.8
O(1)−H(1)···Br(3)	0.936(8)	2.704(10)	3.5877(16)	157.6(12)
O(1)−H(2)···Br(1)	0.940(7)	2.533(8)	3.4627(15)	170.3(16)
160 K				
N(1B)−H(1B)···Br(1)	0.86	2.71	3.375(2)	135.7
N(1B)−H(1B)···Br(6)	0.86	2.86	3.507(2)	133.5
N(3B)−H(3B)···Br(1)	0.86	2.62	3.470(2)	171.5
N(1C)−H(1C)···Br(4)	0.86	2.54	3.399(3)	172.7
N(3C)−H(3C)···O(1)	0.86	1.97	2.823(3)	169.5
N(1A)−H(1A)···O(1)	0.86	2.28	2.958(3)	135.6
N(1A)−H(1A)···Br(5)	0.86	3.01	3.532(3)	121.5
N(3A)−H(3A)···Br(2)	0.86	2.47	3.314(3)	168.6
O(1)−H(1)···Br(3)	0.932(16)	2.52(2)	3.436(2)	167(2)
O(1)−H(2)···Br(2)	0.904(16)	2.82(3)	3.529(2)	136(2)
O(1)−H(2)···Br(1)	0.904(16)	2.87(2)	3.555(2)	134(2)

3.3. Dielectric properties of TIBA

The temperature dependence of the real part of complex electric permittivity, (ε'), along the *a*-axis was measured between 2 kHz and 1 MHz upon cooling (Fig. 4). The phase transition is accompanied by a rapid decrease in electric permittivity ($\Delta\varepsilon' \approx 2$) and a subtle change in dielectric losses (not presented). No dielectric relaxation process is observed whether above or below the transition temperature (212 K). Such a dielectric response close to 212 K indicates that a sudden cessation of motion of dipolar groups (imidazole rings) takes place.

3.4. The phase transition mechanism in TIBA at 212 K

Neat $(C_3N_2H_5)_3SbBr_6 \cdot H_2O$ (TIBA) undergoes discontinuous phase transition at 212/221 K, accompanied by $\Delta S_{tr} = 14.6$ J/mol K. Taking into account only the magnitude of this ΔS_{tr}, the phase transition may be classified as an order–disorder transition. On the other hand, X-ray diffraction on TIBA showed that all atoms are placed in general positions in the disordered phase I. This fact is important in the case of the imidazolium cations because they are expected to contribute to the phase transition mechanism. From the crystallographic point of view, the change in cation dynamics (mainly of the type C imidazole ring) does not lead to a change in crystal symmetry. This agrees with the observed sequence of transitions at 212 K, because we deal with the isostructural phase transition I→II ($P2_1/c \rightarrow P2_1/c$). The ordering of

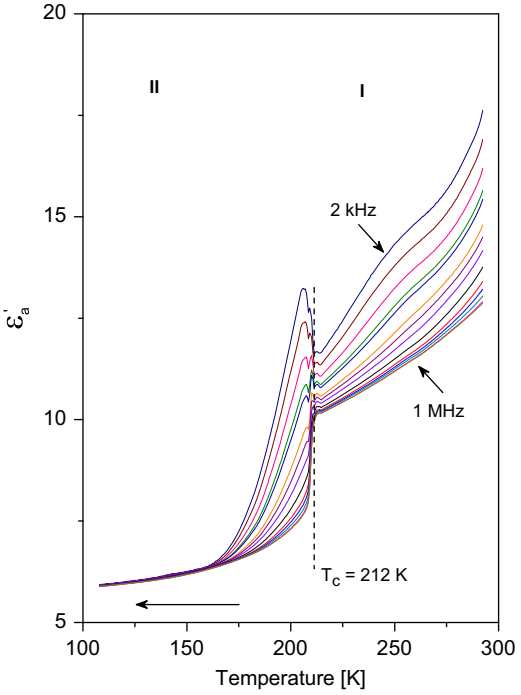

Fig. 4. Frequency dependencies of ε' along the *a*-direction for the single crystal of $(C_3N_2H_5)_3SbBr_6 \cdot H_2O$ upon cooling.

the imidazolium cations of type C contributes to the entropy of transition (ΔS), but it is not the direct reason of the phase transition. In our opinion the phase transition mechanism is governed by the displacive contribution. Detailed analysis of the structural changes through the transition at 212 K showed that the most important changes are connected with the relative displacement of the water molecules with respect to the imidazole rings. Some of the hydrogen bonds exhibit a significant shortening after crossing the phase transition temperature. This effect seems to be directly coupled with a change in the dynamics of type C imidazolium cations.

In conclusion, the phase transition I→II is characterized by two contributions: (i) order–disorder (disorder of cationic substructure), (ii) displacive—relating to a significant reorganization of the hydrogen bond structure (shift of water molecules). The latter contribution prevails in the transition mechanism.

4. Solid-state chemical reaction at 328 K: from $(C_3N_2H_5)_3Sb_2Br_6 \cdot H_2O$ to $(C_3N_2H_5)_5Sb_2Br_{11}$

4.1. Thermal properties (DSC) at high temperatures

It was shown that the DSC traces for two kinds of samples of TIBA, heated/annealed above 330 K, and not heated above 330 K, appeared to be markedly different at low temperatures. It should be emphasized that the phase transition sequence depends on the temperature history of the sample annealed at high temperatures.

The DSC traces of samples that were annealed above 330 K (at 370 K for 30 min) are shown in Fig. 5. Below RT, three phase transitions are found: II↔III at 192/202 K (strong-first order), and III↔IV at 140 K (second order). Above RT, one strong first-order transition (I↔II) is found at 354/351 K. The transition entropy for the I↔II transition amounts to *ca.* 7 J/mol K, and that for the III↔IV transition is close to 3 J/mol K. The next piece of evidence confirming the presence of crystalline $(C_3N_2H_5)_5Sb_2Br_{11}$ in the sample is the fact that the high-temperature phase transition in an originally annealed sample was detected at 354/351 K (heating–cooling), whereas in neat $(C_3N_2H_5)_5Sb_2Br_{11}$ it appeared at 354/352 K [20].

4.2. X-ray powder diffraction phase analysis

High-temperature X-ray powder diffraction analysis confirms anomalies observed in DSC runs. Fig. 6 presents X-ray diagrams for TIBA and $(C_3N_2H_5)_5Sb_2Br_{11}$ crystals measured at different temperatures. Each phase has its own unique powder patterns. Fig. 6(a) presents the powder diagram for as-grown $(C_3N_2H_5)_3SbBr_6 \cdot H_2O$ measured at 298 K. The same sample at 328 K (Fig. 6(b)) displays diffraction peaks that are characteristic of $(C_3N_2H_5)_5Sb_2Br_{11}$ (Fig. 6(c)). Asterisks point to the presence of an additional phase, namely $(C_3N_2H_5)Br$. To ensure that we deal with a new structure, the sample was further heated to 368 K (Fig. 6(d)). The diffraction patterns also happen to be characteristic of the high-temperature phase of $(C_3N_2H_5)_5Sb_2Br_{11}$ (Fig. 6(e)). Heating $(C_3N_2H_5)_3SbBr_6 \cdot H_2O$ from 298 to 328 K results in a change of the diffraction patterns and in the creation of an amorphous phase in the sample. Crystallinity calculations showed that after the chemical reaction 20% of amorphous phase appears.

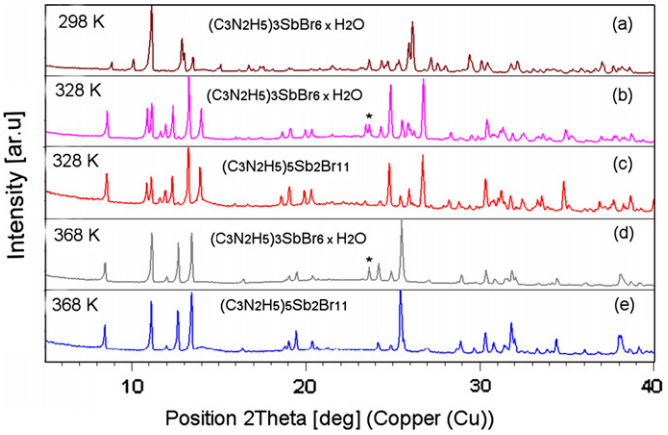

Fig. 6. X-ray diffraction patterns of: (a) $(C_3N_2H_5)_3SbBr_6 \cdot H_2O$ at 298 K. (b) $(C_3N_2H_5)_3SbBr_6 \cdot H_2O$ at 328 K. (c) $(C_3N_2H_5)_5Sb_2Br_{11}$ at 328 K. X-ray diffractograms of both compounds at 328 K are almost identical, additional peaks from $(C_3N_2H_5)Br$ are present in (b) and (d). Further heating of both samples ((d), (e)) lead to transformation to phases possessing exactly the same diffraction peaks.

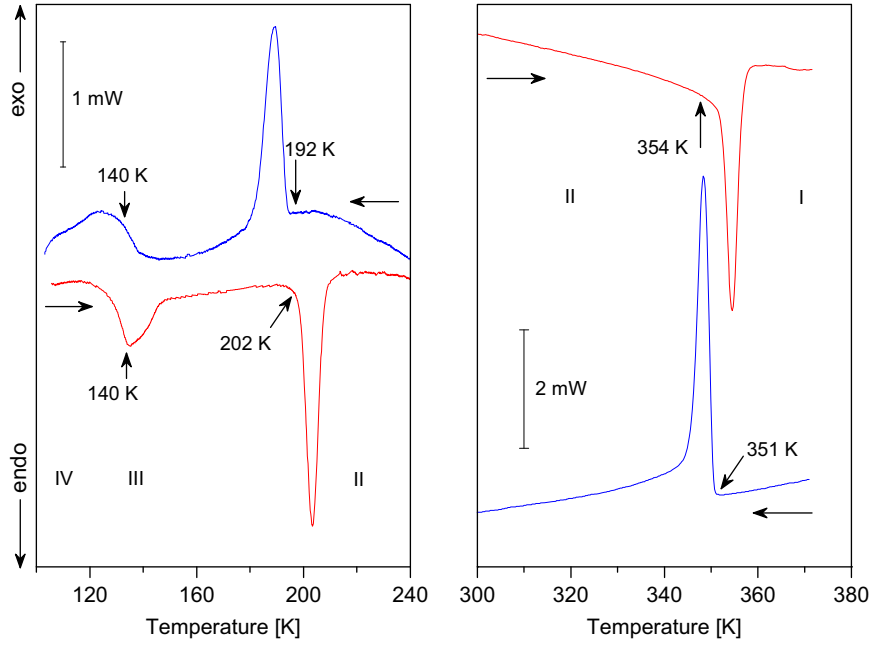

Fig. 5. DSC curves for the $(C_3N_2H_5)_3SbBr_6 \cdot H_2O$ crystal annealed at 350 K for 2 h upon cooling and heating (10 K/min, m=14.3 mg).

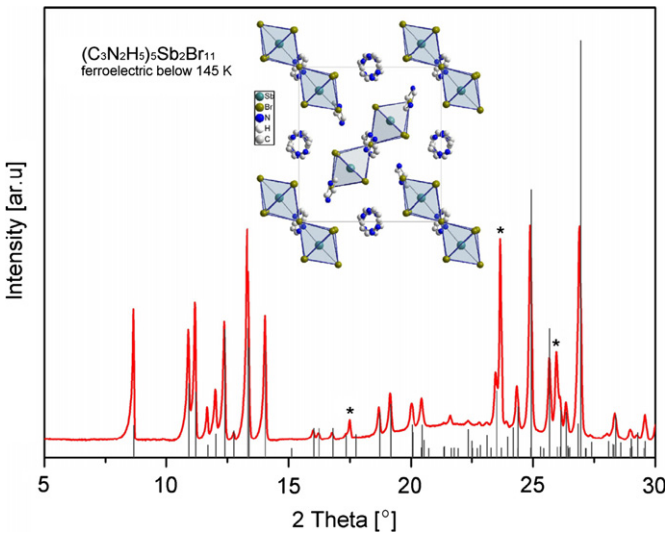

Fig. 7. Powder diffraction diagram for the $(C_3N_2H_5)_3SbBr_6 \cdot H_2O$ sample that was heated at 363 K for 3 h and then cooled to the room temperature. The positions of diffraction patterns characteristic for $(C_3N_2H_5)_5Sb_2Br_{11}$ are marked as lines below the diagram. Asterisks mark the peaks from $(C_3N_2H_5)Br$. The crystal structure of $(C_3N_2H_5)_5Sb_2Br_{11}$ at room temperature (from [20]) is also depicted.

Fig. 7 presents the powder diagram of $(C_3N_2H_5)_3SbBr_6 \cdot H_2O$ that was annealed at 363 K for 3 h. The patterns are characteristic of $(C_3N_2H_5)_5Sb_2Br_{11}$, and almost all peaks are indexed in a monoclinic $P2_1/n$ cell with the following lattice parameters: $a = 9.1399(19)$ Å, $b = 15.150(3)$ Å, $c = 13.969(3)$ Å, and $\beta = 96.19(3)^\circ$ [20]. Peaks marked by asterisks evidence the presence of crystalline $(C_3N_2H_5)Br$ in the measured sample.

4.3. Dielectric properties of annealed sample

The dielectric results obtained for the single-crystal sample of $(C_3N_2H_5)_3SbBr_6 \cdot H_2O$ annealed at 350 K for 2 h appear to be the most unexpected. After passing through 328 K, the single crystal becomes nontransparent and distinctly degraded. Nevertheless, the shape of the sample is kept without any changes and the sample seems to be mechanically stable.

The real part of the complex electric permittivity, ε', measured between 2 kHz and 1 MHz below RT, is shown in Fig. 8. Two distinct dielectric anomalies in the form of jumps in the dielectric permittivity were observed at about 202 K ($\Delta\varepsilon \approx 4-6$) and 192 K ($\Delta\varepsilon \approx 2$). In the case of the original (unannealed) sample of $(C_3N_2H_5)_3SbBr_6 \cdot H_2O$, only one dielectric anomaly was detected, at *ca.* 212 K (see Fig. 4).

We also compared the dielectric properties of annealed $(C_3N_2H_5)_3SbBr_6 \cdot H_2O$ and $(C_3N_2H_5)Br$ between 150 and 250 K during heating (Fig. 9). These two materials revealed quite similar sequences of phase transitions show two dielectric anomalies which undoubtedly correspond to each other (200 and *ca.* 230 K). The lower temperature anomaly was confirmed by DSC but the higher temperature one is invisible. The intermediate phase (between 202 and 230 K) is probably metastable and strongly depends on the scanning rate. DSC measurements were carried out at *ca.* 10 K/min whereas the dielectric ones at *ca.* 0.1–0.3 K/min.

Unexpectedly, the most spectacular dielectric anomaly was detected close to 140 K in $(C_3N_2H_5)_3SbBr_6 \cdot H_2O$ annealed above 330 K (see Fig. 8). In general, this anomaly confirmed for the large number of annealed samples, to a large extent resembles the dielectric function (with significantly smaller dielectric increment) found in the vicinity of the paraelectric–ferroelectric phase transition of $(C_3N_2H_5)_5Sb_2Br_{11}$. Detailed analysis of this characteristic

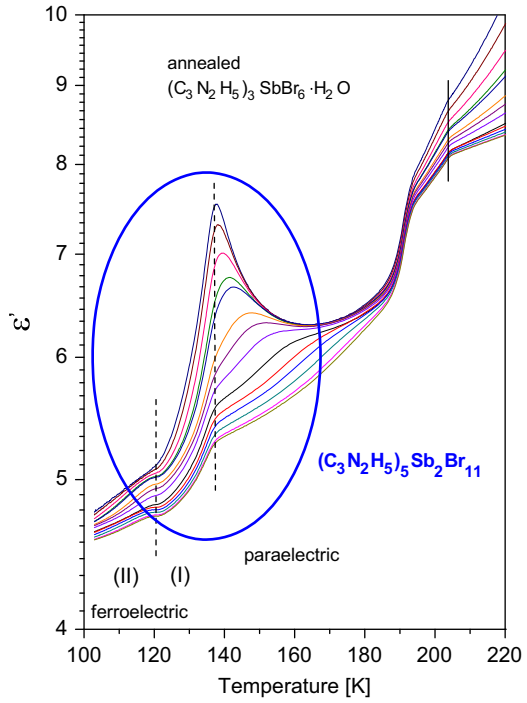

Fig. 8. Real part of the complex electric permittivity, ε', in the vicinity of the paraelectric–ferroelectric phase transition. Marked area (blue line) corresponds to the ferroelectric phase of $(C_3N_2H_5)_5Sb_2Br_{11}$. (For interpretation of the references to colour in this figure legend, the reader is referred to the web version of this article.)

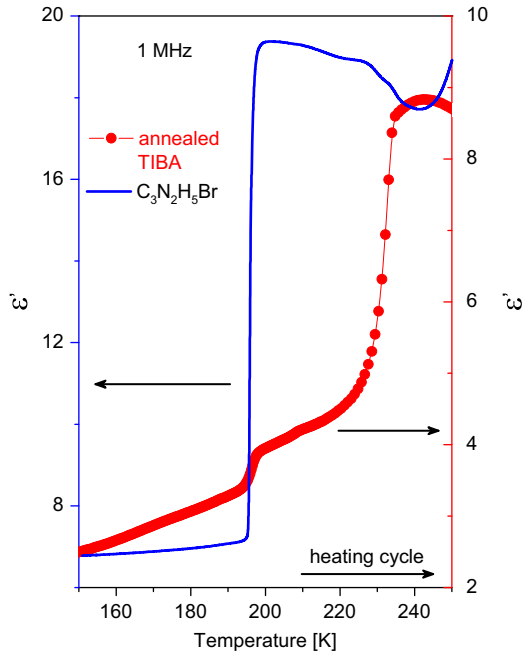

Fig. 9. Real part (ε') of the complex electric permittivity for the pressed powder pellet of $(C_3N_2H_5)Br$ (solid line), and annealed sample of $(C_3N_2H_5)_3SbBr_6 \cdot H_2O$ (circles).

allowed us to the conclusion that the dynamic dielectric properties of an annealed sample in the vicinity of 140 K may be treated as a "fingerprint" of a neat $(C_3N_2H_5)_5Sb_2Br_{11}$ derivative. The analysis of the dynamic dielectric properties of an "annealed" sample around the 140 K transition are presented in supplementary materials.

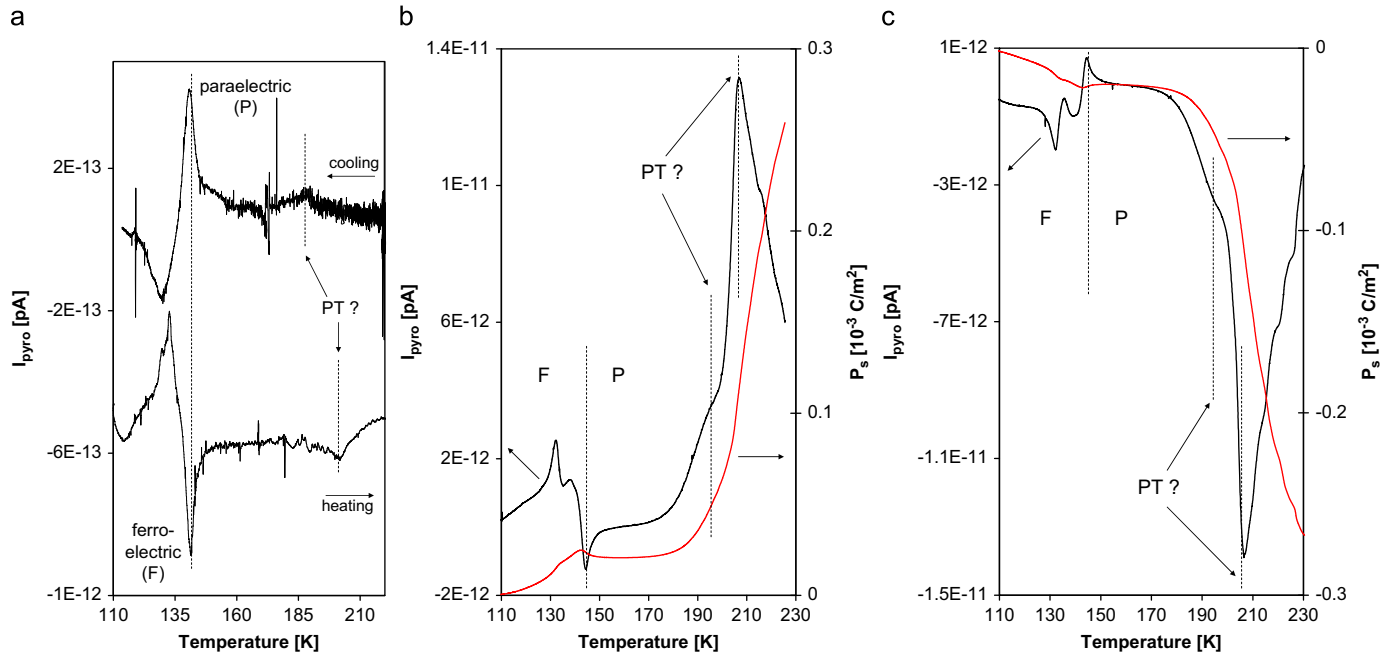

Fig. 10. (a) Pyroelectric current measured on cooling and heating for the annealed sample of $(C_3N_2H_5)_3SbBr_6 \cdot H_2O$ without the poling dc electric field, (b) and (c) the pyroelectric current (black line) and corresponding spontaneous polarization (red line) for the annealed sample of $(C_3N_2H_5)_3SbBr_6 \cdot H_2O$ which was poled with +1 and -1 kVcm^{-1} dc electric field, respectively. (For interpretation of the references to colour in this figure legend, the reader is referred to the web version of this article.)

4.4. *Pyroelectric measurements*

To verify the polar nature of the created crystalline powdered $(C_3N_2H_5)_5Sb_2Br_{11}$ derivative in an annealed sample of TIBA, we decided to perform pyroelectric measurements. We made two kinds of such measurements: (i) measurements of the pyroelectric current without bias poling dc electric field of the sample; and (ii) measurements of the pyroelectric current after bias poling dc electric field. For the measurements without poling, the current was recorded on cooling, starting from 250 down to 110 K, and then on heating for the same temperature range. The results are shown in Fig. 10(a). It is clearly seen that the pyroelectric current arises close to 140 K, and this process is reversible during the cooling and heating cycles. For the other set of measurements, the pyroelectric current was measured after poling dc electric field the crystal while cooling from 230 K to about 100 K. The dc electric field was equal to +1 kV cm^{-1}. Then the bias pyroelectric current (I_{pyro}) was measured during the heating cycle. The same procedure was applied after poling the crystal by a negative dc electric field (-1 kV cm^{-1}). The changes in spontaneous polarization (ΔP_s) as a function of temperature are shown in Fig. 10(b) and (c). It is clear that the spontaneous polarization (P_s) is reversed by the external dc electric field in the vicinity of 140 K. This is a crucial piece of evidence for ferroelectric properties below 140 K. This pyroelectric experiment confirms that in the annealed sample of $(C_3N_2H_5)_3SbBr_6 \cdot H_2O$, which is treated as a multiphase material, there appears a ferroelectric order resulting from $(C_3N_2H_5)_5Sb_2Br_{11}$ crystallites.

5. Discussion

The phase situation in neat $(C_3N_2H_5)_3SbBr_6 \cdot H_2O$ is quite clear. The single-crystal X-ray diffraction and thermal studies of TIBA revealed one isostructural phase transition at 212/221 K. The molecular mechanism of this transition seems to be rather complex; thus, two contributions were considered: (i) an order–disorder one and (ii) a displacive one. The order–disorder mechanism is justified by a significant transition entropy effect ($\Delta S_{tr} = 14.6$ J/mol K) resulting from the disordered imidazolium cations. On the other hand, all the atoms of the imidazole ring are placed in general positions; thus, the order of the cations below 212 K does not lead to a change in the space group. The second possibility, a displacive mechanism, is due to the significant shift of the water molecules in the lattice and substantial changes in the hydrogen bond configuration through the phase transition at 212 K. The water molecules play a major role in the displacive phase transition mechanism.

The most interesting feature of the compound under investigation at higher temperatures is an unprecedented in situ solid-state direct chemical reaction leading from non-polar crystal $(C_3N_2H_5)_3SbBr_6 \cdot H_2O$ to crystalline ferroelectric $(C_3N_2H_5)_5Sb_2Br_{11}$. Such a type of chemical reaction is reported for the first time in the halogenoantimonates(III) or halogenobismuthates(III) that have been studied so far.

The question arises which crystalline phases can really exist in the solid state after the annealing of $(C_3N_2H_5)_3SbBr_6 \cdot H_2O$ (TIBA) at temperatures above 330 K. The proposed chemical reaction given by Eq. (2) is not based strictly on the thermogravimetric measurements but results from the analysis and considerations of various physical properties of the materials presented in this paper. The loss of sample mass with temperature is continuous and rather small, not characteristic of such a drastic type of chemical reaction. We can only state that the final crystalline products of the chemical reaction are still present in the powdered sample even at high temperatures, up to 450 K. Imidazolium bromide is strongly hygroscopic; thus, the water molecules are bonded in the sample even at higher temperatures, and only some part of the water is continuously removed before reaching the phase transition at 354 K. Taking into account the TGA, X-ray, and dielectric results, we can state that after TIBA is annealed, above 328 K the sample may be treated as a crystalline multiphase system consisting of at least three crystalline phases: $(C_3N_2H_5)_5Sb_2Br_{11(s)}$, $(C_3N_2H_5)Br_{(s)}$ and traces of $(C_3N_2H_5)_3SbBr_6 \cdot H_2O$. All the phases are in equilibrium with $H_2O_{(liquid)}$. Fig. 11 illustrates the phase situation of the four

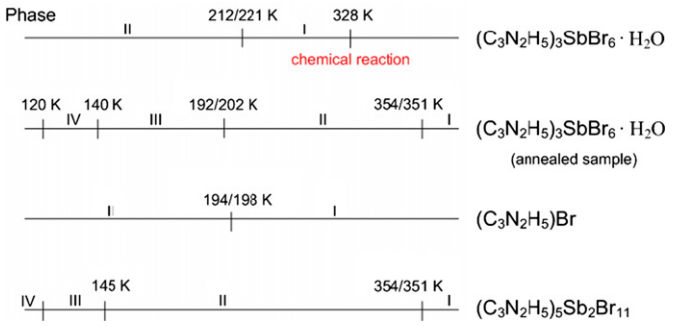

Fig. 11. The phase diagram of the four compounds: $(C_3N_2H_5)_3SbBr_6 \cdot H_2O$, $(C_3N_2H_5)_5Sb_2Br_{11}$, $C_3N_2H_5Br$, and annealed $(C_3N_2H_5)_3SbBr_6 \cdot H_2O$, comparing their phase transition sequences.

compounds considered: $(C_3N_2H_5)_3SbBr_6 \cdot H_2O$, $(C_3N_2H_5)_5Sb_2Br_{11}$, $C_3N_2H_5Br$, and annealed $(C_3N_2H_5)_3SbBr_6 \cdot H_2O$, comparing their phase transition sequences:

The above was determined on the basis of thermal methods like DSC and dilatometry. The diagram clearly shows that the sample of $(C_3N_2H_5)_3SbBr_6 \cdot H_2O$ after the chemical transformation reveals most of the phase transitions that appear separately in all the neat compounds now existing as various percolating crystalline phases. The probable constitution of the annealed sample was additionally confirmed by the X-ray powder diffraction method. The most valuable result of the present studies is the fact that we succeeded in obtaining a new crystalline ferroelectric material using an in situ solid-state direct chemical reaction, where the starting substrate was a different chemical compound in the solid state. The existence of crystallites of $(C_3N_2H_5)_5Sb_2Br_{11}$ was confirmed by dielectric and pyroelectric methods. The dielectric response (critical slowing down) approaching 140 K and reversible spontaneous polarization below 140 K are a "fingerprint" of the known ferroelectric $(C_3N_2H_5)_5Sb_2Br_{11}$.

Acknowledgment

This work was supported by the Polish State Committee for Scientific Research (project register No N N204 147837).

Appendix A. Supplementary material

Crystallographic data for the structures reported in this paper (excluding structure factors) have been deposited with the Cambridge Crystallographic Data Centre, CCDC no. 755624-55627. Copies of this information may be obtained free of charge from the Director, CCDC, 12 UNION Road, Cambridge CB2 1EZ, UK (fax: +44 1223 336033; e mail: deposit@ccdc.cam.ac.uk or http://www.ccdc.cam.ac.uk).

Appendix B. Supplementary data

Supplementary data associated with this article can be found in the online version at doi:10.1016/j.jssc.2010.10.020.

References

[1] J. Zyss, Molecular Nonlinear Optics: Materials, Physics and Devices, Academic Press, New York, 1993.
[2] F. Agullo-Lopez, J.M. Cabrera, F. Agullo-Rueda, Electrooptics: Phenomena, Materials, and Applications, Academic Press, New York, 1994.
[3] R.E. Newnham, Structure and Property Relations, Academic Press, New York, 1975.
[4] G.R. Desiraju, Crystal Engineering: The Design of Organic Solids, fourth ed., Elsevier, New York, 1989.
[5] J.-L. Lehn, Supramolecular Chemistry: Concepts and Perspectives, VCH, New York, 1995.
[6] T.J. Marks, M.A. Ratner, Angew. Chem. 34 (1995) 155–173.
[7] H.Y. Ye, D.W. Fu, Y. Zhang, W. Zhang, R.G. Xiong, S.D. Huang, J. Am. Chem. Soc 131 (2009) 42–43.
[8] M. Szafrański, A. Katrusiak, Phys. Rev. B 73 (2006) 134111-1–134111-8.
[9] L. Sobczyk, R. Jakubas, J. Zaleski, Pol. J. Chem. 71 (1997) 265–300.
[10] G. Xu, Y. Li, W. Zhou, G. Wang, X. Long, L. Cai, M. Wang, G. Guo, J. Huang, G. Bator, R. Jakubas, J. Mater. Chem. 19 (2009) 2179–2183.
[11] W. Bi, N. Leblanc, N. Mercier, P. Auban-Senzier, C. Pasquier, Chem. Mater. 21 (2009) 4099–4101.
[12] M. Hall, M. Nunn, M.J. Begley, D.B. Sowerby, J. Chem. Soc. Dalton Trans. (1986) 1231.
[13] M. Nunn, A.J. Blake, M.J. Begley, D.B. Sowerby, Polyhedron 17 (1998) 4213.
[14] J. Zaleski, C. Pawlaczy, R. Jakubas, H.-G. Unruh, J. Phys.: Condens. Matter 12 (2000) 7509–7521.
[15] M. Bujak, J. Zaleski, Cryst. Eng. 4 (2001) 241–252.
[16] P. Carpentier, J. Lefebvre, R. Jakubas, Acta Crystallogr. Sect. B Struct. Sci. 51 (1995) 167–174.
[17] P. Carpentier, P. Zieliński, J. Lefebvre, R. Jakubas, J. Phys.: Condens. Matter 102 (1997) 403–414.
[18] J. Jóźków, G. Bator, R. Jakubas, A. Pietraszko, J. Chem. Phys. 114 (2001) 7239–7246.
[19] A. Piecha, A. Białońska, R. Jakubas, J. Phys.: Condens. Matter 20 (2008) 325224 (9pp).
[20] A. Piecha, A. Pietraszko, G. Bator, R. Jakubas, J. Solid State Chem. 181 (2008) 1155–1166.
[21] S. Chaabouni, S. Kamoun, A. Daoud, T. Jouini, J. Chem. Crystallogr. 27 (1997) 401–404.
[22] S. Chaabouni, S. Kamoun, J. Jaoud, Mat. Res. Bull. 33 (1998) 377–388.
[23] S. Nasri, F. Zouari, H. El Feki, J. Chem. Crystallogr. 38 (2008) 729–732.
[24] F. Lazarini, Acta Crystallogr. C 43 (1987) 637–638.
[25] A. Ouasri, H. Jeghnou, A. Rhandour, M.C. Dhamelincourt, P. Dhamelincourt, A. Mazzah, P. Roussel, J. Raman Spectrosc. 36 (2005) 791–796.
[26] F. Lazarini, Acta Crystallogr. C 41 (1980) 1617–1619.
[27] H. Zhang, L. Fang, Acta Crystallogr. E 60 (2004) m1819–m1821.
[28] I.M. Vezzosi, L.P. Battaglia, A.B. Corradi, Inorg. Chim. Acta 89 (1984) 151–155.
[29] Oxford Diffraction, CrysAlis CCD and CrysAlis RED, ver. 171.32.6. Oxford Diffraction Ltd. Abingdon, England, 2007.
[30] G.M. Sheldrick, SHELX. Program for the Solution and Refinement of Crystal Structures, University of Göttingen, Germany, 1997.